Applied Physics B (2022) 128:34
https://doi.org/10.1007/s00340-022-07756-4

Applied Physics B
Lasers and Optics

Understanding all-optical switching at the epsilon-near-zero point: a tutorial review

Colton Fruhling[1] · Mustafa Goksu Ozlu[1] · Soham Saha[1] · Alexandra Boltasseva[1] · Vladimir M. Shalaev[1]

Received: 10 November 2021 / Accepted: 10 January 2022 / Published online: 29 January 2022

Abstract
Epsilon-near-zero (ENZ) materials that operate in the spectral region where the real part of the permittivity crosses zero have recently emerged as a promising platform for all-optical switching because of the large, optically induced reflectance and transmittance modulation they offer at ultrafast speeds. To gain insights into the ENZ modulation, this study focuses on the reflectance and transmittance modulation of commonly used ENZ switching schemes and applies an analytical framework both for intraband and interband pumping. We consider the effects of the wavelength, the angle, and the probe polarization on the modulation amplitude for different configurations, specifically highlighting the locations of the maximum reflectance/transmittance modulation and the maximum refractive index modulation, which often occur at different wavelengths around the ENZ point. We find that the maximum modulation, while proximal to the ENZ point, can occur away from the ENZ point and even slight deviations can result in seemingly anomalous modulation behavior. The occurrence of resonances at the ENZ region for ultrathin films further increases the modulation strength. This work paves the path for practical and effective all-optical modulation approaches employing ENZ materials, and will help design the best experimental configurations for future material studies and nonlinear optical experiments employing ENZ materials.

1 Introduction

One of the longstanding goals of photonics is to control the flow of light using all-optical excitation that is typically achieved via nonlinear light–matter interactions. Since all-optical control is free from many inherent resistance–capacitance delays in electrical control, there is a great effort for ultrafast optics on the picosecond timescale to compete and surpass current electronic technologies. As a result, the availability of CMOS compatible materials which exhibit a significant refractive index change under low illuminations with a picosecond-to-femtosecond response time is crucial for the realization of many on-chip nonlinear applications. However, the nonlinear response of most materials is generally feeble and only considered as a perturbation to linear effects. The common strategy to overcome this hurdle is to use long interaction lengths or intense laser illumination, which is not desirable for practical applications. This has prompted extensive research to develop new platforms that show strong nonlinearities.

In recent years, the so-called epsilon-near-zero (ENZ) materials, with a spectral region where the real part of the permittivity ϵ crosses zero, have emerged as one of the most promising platforms for all-optical switching. Naturally occurring homogeneous ENZ material comprises metals [1–4] and semiconductors [5–7], and ENZ regions may also be engineered with metamaterials [8–16]. They have been shown to exhibit exotic behaviors such as photon tunneling [10, 16–18], highly directional radiation [19–21], cloaking [22], and perfect absorption [23–25]. Additionally, due to the diverging phase velocity and electric field enhancements, ENZ materials have been used to significantly enhance nonlinear responses [6–9, 26–29] described in the recent reviews [30–34].

One promising homogeneous ENZ material class is transparent conducting oxides (TCOs). TCOs such as doped oxides of zinc or indium are advantageous, because their ENZ regime is located in the telecom range (1.3–1.5 μm) and they exhibit low losses (small imaginary part of the electric permittivity) [35, 36] while offering an ultrafast response time on the scale of femtoseconds at the ENZ [5,

✉ Colton Fruhling
cfruhlin@purdue.edu

[1] School of Electrical and Computer Engineering, Birck Nanotechnology Center and Purdue Quantum Science and Engineering Institute, Purdue University, West Lafayette, IN, USA

37, 38]. Importantly, the optical properties of TCOs, including losses and the location of the ENZ region, can be effectively tailored by altering the growth/deposition conditions, thickness, and dopant ratio [39–43]. By utilizing TCOs as ENZ materials, ultrafast switching [5, 44], enhanced third harmonic generation [45–47], resonance pinning [48–51], optical time reversal [52], and adiabatic frequency conversion [53–55] have been demonstrated.

In this paper, we focus on the dynamic behavior of a homogeneous ENZ medium under optical modulation at the maximum modulation, that is, at maximum pump-probe overlap. Using the Drude model, we explore how an optical pump affects the optical properties of a TCO film by modulating the plasma frequency and damping rate. These effects are framed in the context of ultrafast all-optical switching experiments. The paper consists of four parts. The first part focuses on the theoretical study of the modulation of the optical properties. The second and third parts analyze how the reflectance and transmittance are modulated under intraband and interband pumps for optically thick and thin ENZ layers, respectively. The last section discusses the effects resulting from changing the damping. Understanding the effects of the modulated plasma frequency and the Drude-damping coefficient provides the foundations for setting up transient pump-probe experiments for practical ENZ studies.

The goal of this review paper is to act as a primer, going through common experimental configurations and ENZ schemes, particularly for all-optical switching experiments. This will help design the best configurations for pump-probe spectroscopy to extract material dynamics. These configurations also form the basis for more complex experiments such as time refraction [55], negative refraction in time-varying media [56], and photonic time crystal design [57]. Understanding all-optical modulation through interband and intraband pumping serves as the first step to developing more complex experiments involving the dynamic modulation of epsilon-near-zero materials.

2 Theoretical model

ENZ materials have certain beneficial properties that lead to the enhancement of nonlinear response. First, since the real part of the ENZ material's permittivity crosses zero, the normal component of the electric field is enhanced at the interface. This can be understood by examining the charge-free boundary conditions of the normal electric field component at the interface $\varepsilon_1 E_1^{\perp} = \varepsilon_2 E_2^{\perp}$, where the subscripts denote differing materials. If $\varepsilon_2 \to 0$, there is a large enhancement of $E_2^{\perp}$ at the interface. This is especially important for thin films, and thus, our discussion is focused mainly on TM modes. Second, the diminishing group velocity at ENZ gives rise to the so-called slow light effect [58–60]. Light–matter interactions are highly enhanced due to the extended interaction time. Therefore, it is possible to obtain very high modulations in the linear refractive index with small changes in the material properties.

All-optical switching in ENZ materials is driven by modulating the refractive index, which in a non-magnetic material is given by $n = \sqrt{\varepsilon}$. The change of the refractive index is then $\Delta n \propto \Delta\varepsilon/\sqrt{\varepsilon}$, which indicates that large changes in the index are expected near the ENZ point even for a small change in the permittivity [32] (Fig. 1b). This is one of the key advantages of using ENZ materials for all-optical switching [5, 7, 61, 62]. However, as seen in Fig. 1b, the modulation of the refractive index is largest near the ENZ point but not exactly at it and the peak changes position with different levels of modulation. This is due to the nonzero imaginary permittivity and the shifting real permittivity with increasing pump fluence.

The permittivity can be modulated by optically pumping the material. We study the effects of optical pumping on ENZ materials using the Drude model [63, 64] that describes the permittivity of free electrons and can model reasonably well electrons in the conduction band. The permittivity is described as

$$\varepsilon = \varepsilon_{\mathrm{Re}} + i\varepsilon_{\mathrm{Im}} = \varepsilon_{\infty} - \frac{\omega_{\mathrm{p}}^2}{\omega^2 + i\Gamma_0\omega} \tag{1}$$

$$\varepsilon_{\mathrm{Re}} = \varepsilon_{\infty} - \frac{\omega_{\mathrm{p}}^2}{\omega^2 + \Gamma_0^2} \tag{2}$$

$$\varepsilon_{\mathrm{Im}} = \frac{\omega_{\mathrm{p}}^2\Gamma_0}{\omega\left(\omega^2 + \Gamma_0^2\right)} \tag{3}$$

$$\omega_{\mathrm{p}}^2 = \frac{Ne^2}{\varepsilon_0 m^*}. \tag{4}$$

In Eq. (1), ε_∞ is the response in the high-frequency limit, ω_{p} is the plasma frequency of the electrons in the conduction band, and Γ_0 is the damping rate of plasma oscillations. The real and imaginary parts are given by Eqs. (2) and (3), respectively. In Eq. (4), for the plasma frequency, N is the electron number density, e is the charge, and ε_0 is the permittivity of free space. The effective mass m^* is defined as $m^* = \alpha m_0$, where α is a scalar quantity and m_0 is the mass of an electron in free space. If we assume a relatively small damping factor (which is valid for many TCOs at the ENZ point), the ENZ point occurs at $\omega_{\mathrm{ENZ}} \approx \omega_{\mathrm{p}}/\sqrt{\varepsilon_\infty}$. Therefore, one can use the plasma frequency to control the ENZ point and thus to control the amplitude and sign modulation of reflectance

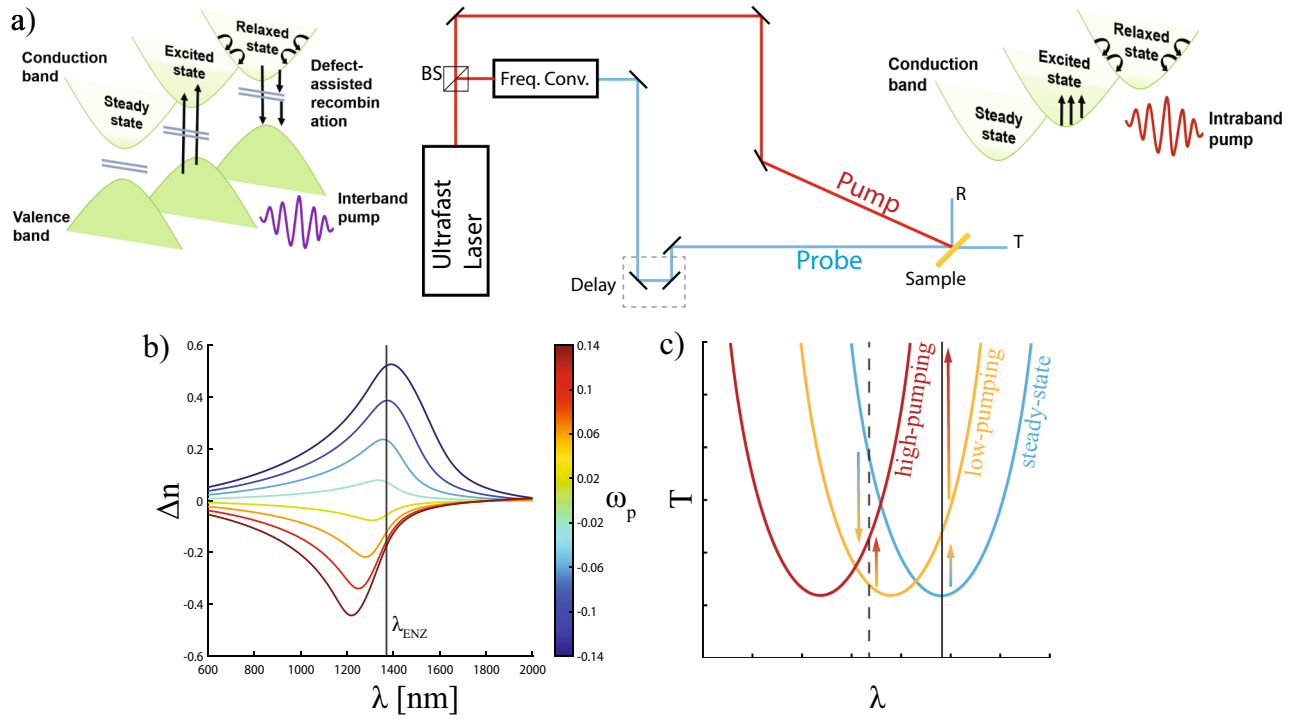

Fig. 1 **a** A typical experimental setup for optical pump-probe experiments. An ultrafast laser pulse is generated and used to create a probe beam at the desired frequency. Schematics for interband and intraband pumping are shown on the sides. **b** The change in index of refraction for different relative changes in the plasma frequency $\Delta\omega_p/\omega_p$ near the ENZ point (denoted with vertical line). See Table 1 for the initial parameters of this plot. **c** A schematic of a dip in transmission as material is changed due to optical pumping. Two observation points are noted with vertical solid and dashed lines. The arrows indicate the direction of change seen by the observer. At the wavelength indicated by the solid line, increasing pump results in increasing the transmission. However, under the same conditions, a probe at the dashed line observes first a decrease in transmission at low pump intensities, followed by an increase at higher intensities

and transmittance. This also gives a means to control the spectral position of the resonance for thin ENZ films.

In TCOs, an optical pulse changes the plasma frequency (ω_p) by either changing the number density of free electrons (N) or the average effective mass (m^*). The band-gap energy supplies a natural distinction between two regimes of optical manipulation of the plasma frequency. For pump photon energies higher than the band gap, electrons are promoted from valence to conduction band, which we call interband transitions (left Fig. 1a). Interband transitions naturally add more electrons to the conduction band and thus increase the plasma frequency [37, 65]. For photon energies less than the band gap, intraband transitions move electrons to higher energies, (right Fig. 1a) where due to the non-parabolic nature of the band structure, the effective mass is increased [66–68]. Thus, a decrease in the plasma frequency is expected [7, 37, 62, 63, 69]. The changes to the optical properties happen on the sub-picosecond timescale. Eventually, the electrons either cool down (in case of intraband pumping) or recombine with holes in the valence band, and the material returns to its original state (in case of interband pumping) (Fig. 1a).

The damping factor in TCOs is also modulated by optical pumping. The rate of collisions between free electrons is described by the damping factor Γ_0, and depends on the number density of electrons, which is increased by interband pumping. The damping affects the ENZ point, red-shifting it for larger values of Γ_0, and contributes to the width of optical resonances (see Sect. 5).

The center of Fig. 1a illustrates the conventional transient pump-probe experiment. In many experiments involving TCOs, the pump is a Ti–sapphire laser at the fundamental wavelength (~ 800 nm), or is frequency-converted by passing through a nonlinear crystal or an optical parametric amplifier. The probe pulse is a femtosecond pulse close to the ENZ wavelength of the material. The sources can vary depending on the type of the experiment, the kind of excitation targeted, and the ENZ point of the materials being investigated. The optical pump generates (interband) or excites (intraband) free carriers in the conduction band of a material, causing the electric permittivity and the refractive index to change. The probe pulse then measures changes in reflectance, transmittance, or both.

The measured response depends on the pump-pulse duration (10–100 fs), the probe-pulse duration (10–100 fs), and the material relaxation (typically ps-ns). The changed reflectance/transmittance measured at a specific pump-probe delay is generally an 'average' response during the probe's temporal pulse-width which is short compared to the material relaxation. Under that assumption, our calculations of the dynamic changes measured by the probe pulse can be carried out with a static calculation. More complicated models have been employed that, for example, take into account the relaxation of the material using a two-temperature model [7, 68].

Intuitively, one might expect the change in the transmittance or the reflectance of a material at a particular wavelength to be monotonic. For example, an increasing interband pump generates free carriers, making the material more metallic, thereby decreasing the transmittance at longer wavelengths, and increasing the reflectance. However, we show that ENZ facilitated resonances—especially for thin films—complicate this intuitive picture. The reflectance and transmittance dynamics can exhibit non-monotonic trends as the pump intensity is increased. As shown in Fig. 1c, the transmittance measured at one particular wavelength can be monotonically increasing, while at other wavelengths, it can first decrease and then increase. This is experimentally relevant when measuring at the steady-state ENZ point, since the minimum of transmittance or reflectance may not occur at the exact ENZ point. We investigate the monotonicity of modulation for different pump-probe configurations in the subsequent sections of this tutorial.

The above analysis describes the physical framework for all-optical switching. However, we also need metrics to compare different configurations. An optical switch should be judged on its modulation depth between high and low states and the amount of pumping required to initiate switching. The switching is realized in the reflectance and transmittance changes which we scale to the incident power of the probe beam. Therefore, the switch with the best contrast will have an absolute change in reflectance or transmittance close to one and will have a relative change much greater than one. We now explore standard experimental configurations utilizing the concepts covered in this section. First, we discuss cases of optically thick layers of ENZ material and then move on to thin cases.

3 Semi-infinite (thickness $\sim \infty$) and optically thick (thickness $\sim \lambda$) ENZ films

The first experimental configuration to examine is the interface between a semi-infinite ENZ material and vacuum. The interaction between optical pump and ENZ is modeled using the Transfer Matrix Method (TMM) [71]. TMM has been employed both for theoretical analysis [72] and for verifying experimental works [73]. For all examples discussed below, unless stated otherwise, we use the initial parameters given in Table 1 for the ENZ material. Interband and intraband pumping are introduced by relative changes to the plasma frequency.

The TMM models reflectance, transmittance, and absorptance. The steady-state reflectance of a semi-infinite ENZ material (Fig. 2a) generally increases with increasing wavelength across the ENZ point (vertical solid black line), as the material transitions from dielectric to metallic. Intraband pumping decreases the plasma frequency, thus raising the ENZ point and shifting the dielectric–metallic transition to higher wavelengths. The absolute modulation of the TM polarized reflectance $\Delta R_{\mathrm{TM}} = R_{\mathrm{modulated}} - R_{\mathrm{steady\ -\ state}}$ (Fig. 2b) decreases to the right of the steady-state ENZ point as the spectrum shifts. The modulation is greatest near the ENZ point where the dielectric–metallic transition occurs.

As with any semi-infinite case, common optical phenomena such as the Brewster angle and the critical angle for total reflection are apparent. The Brewster angle described by $\theta_{\mathrm{B}} = \tan^{-1}(n_{\mathrm{ENZ}}/n_{\mathrm{vac}})$, curls from near the ENZ wavelength to approximately the 60° mark. This is the angle where tangential components of the TM polarized incident and transmitted wave exactly match at the boundary, and thus, there is no reflected TM wave (impedance matching condition is met). The total reflection angle is described by $\theta_{\mathrm{c}} = \sin^{-1}\left(n_{\mathrm{ENZ}}/n_{\mathrm{vac}}\right)$, which for our example occurs between 25° and 90°. Since the refractive index of the ENZ medium is complex due to absorption, the Brewster and the critical angle do not have their traditional meanings [74] derived for real refractive index; however, the effects can still be seen (Fig. 2) [75, 76]. For TM polarization, ENZ point shift induces the largest relative reflectance change $\Delta R_{\mathrm{TM}}/R_{\mathrm{TM}}$ along the Brewster angle where the steady-state reflectance is nearly zero (Fig. 2c). Because of the near zero reflectance at the Brewster angle, small changes in the absolute reflectance can be amplified into large relative changes, a technique utilized in extracting the carrier dynamics of materials through pump-probe

Table 1 Optical properties of a hypothetical ENZ material described by Eq. (1)

Drude model parameters (unpumped)	Value
ε_∞	3
ω_{p}	2.4×10^{15} rads/s
f_{p}	3.8×10^{14}Hz
Γ_0	2.4×10^{13}Hz
λ_{ENZ}	1358 nm

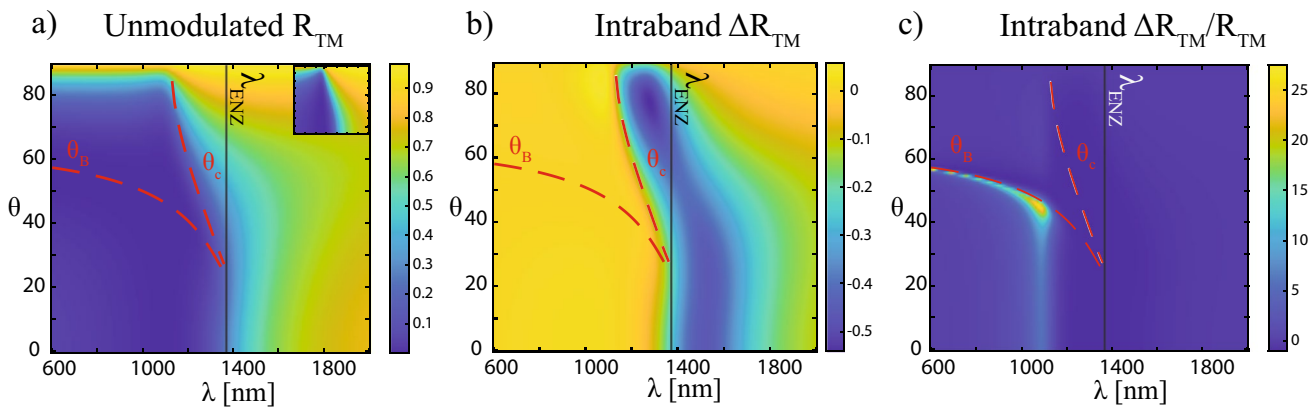

Fig. 2 **a** The unmodulated reflectance of TM polarized light from a semi-infinite ENZ material. Inset: reflectance of TE polarized light. **b** absolute change in reflectance for intraband pumping ($\Delta\omega_p/\omega_p = -0.12$). **c** The relative change in reflectance for the same conditions as **b**. The black vertical line is the unmodulated ENZ point. This is consistent for all similar figures. The red dashed lines are the Brewster θ_B and critical θ_c angles

spectroscopy. However, for all-optical switching, larger changes in the absolute reflectivity are desired.

These effects also are observed in the more practical case of optically thick ENZ layers (Fig. 3). Additionally, multiple reflections between surfaces results in the well-known Fabry-Pérot resonances for wavelengths smaller than the ENZ point. We consider a 900 nm ENZ film deposited on glass ($n_{glass} = 1.5$) and interfacing with vacuum on the other side. The 900 nm thickness was chosen, so that Fabry-Pérot resonances are observed in Fig. 3. The increasing interaction between surfaces also leads to a larger absorption at the ENZ point attributed to the electric field enhancement.

Clearly, these configurations are capable of optical switching as we can see modulation on the order of $\Delta R_{TM} \sim 0.5$. The single step-like transition from non-reflecting to reflecting allows for a broadband optical switch that can be operated with both interband and intraband pumping. The relative change in reflection, however, is relatively small because of the large wavelength range over which the dielectric–metallic transition occurs leaving room for improvement. Even still, such optically thick configurations have been tested with great success.

For example, Kinsey et al. [5] demonstrated picosecond amplitude modulation in optically thick aluminum-doped zinc oxide with an interband pump, while Clerici et al. [37] showed that even faster modulation is possible by combining both interband and intraband pumps. Modulation of the Fabry-Pérot modes has also been observed for example in Yttrium-doped cadmium oxide (CdO) by Saha et al. [40]. In telecommunication wavelengths where the optically thick CdO film is dielectric, moderate transmittance modulations of around 4% were observed. On the other hand, for the same film near the ENZ in the mid-infrared regime, a similar pump fluence showed reflectance modulations of 135%, further underpinning the importance of ENZ induced modulation for lithography-free optical switching.

These configurations can also be used to study the optical properties of materials by performing pump-probe spectroscopy near their ENZ regime. The large changes in the relative reflectance minimum near the ENZ point makes such experiments quite useful for extracting otherwise hidden dynamics in materials. In such experiments, materials are pumped with a high-intensity laser pulse and a lower intensity probe pulse extracts the dynamics. This approach is particularly fruitful at the ENZ point where small changes in the index due to carrier dynamics are amplified.

For example, titanium nitride, a refractory ceramic used for many on-chip and hot-electron applications [70, 77], has an ultrafast electron–phonon response time, which was not apparent in pump-probe spectroscopy experiments performed on it with a probe far from its ENZ value[70]. However, subsequent experiments on TiN and ZrN performed near their respective ENZ points showed this sub-picosecond relaxation time quite clearly, making a strong case for performing pump-probe experiments for material characterization near the materials' ENZ points [61].

4 Thin ENZ films

As the thickness of the ENZ layer decreases beyond the skin depth, the non-radiative surface modes on the upper and lower boundaries start to couple and split into symmetric (long-range) and antisymmetric (short-range) modes [78]. If the film thickness is further reduced, these two modes become even more distinctive, and the symmetric mode forms a flat dispersion curve at the ENZ spectral region called the ENZ mode. The flat dispersion of the ENZ

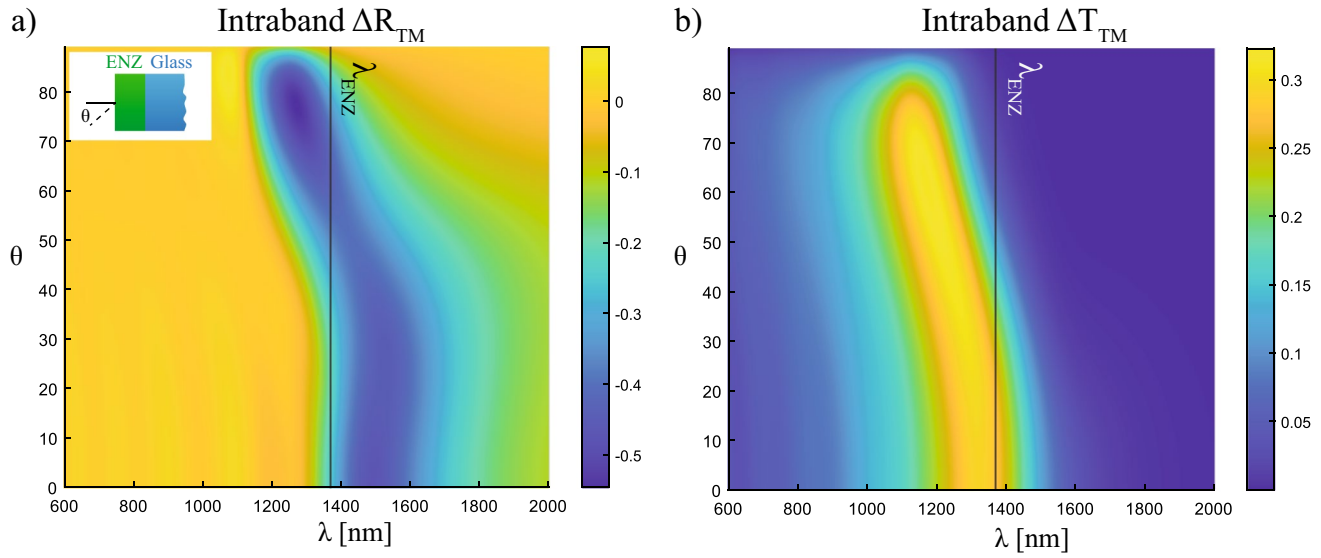

Fig. 3 Modulated ($\Delta\omega_p/\omega_p = -0.12$) TM reflectance **a** and TM transmittance **b** from an ENZ material pumped with intraband laser. The inset of **a** shows the experimental configuration of the ENZ deposited on a glass substrate. The thickness of ENZ material is 900 nm. Fabry–Pérot modes can be seen in the lower left (small wavelength and small incident angle)

mode implies a reduction of the group velocity that is often referred to in slow light schemes [58–60]. Additionally, there is a mode in the radiative region around the ENZ point known as the Ferrell–Berreman (FB) mode [79–81]. When light couples into any of these modes, a large absorptance (reflectance/transmittance) peak (dip) is observed. Optical pumping is then used to shift the peak (dip) resulting in giant reflectance or transmittance modulations due to the narrow resonant features (Fig. 1c). We separate the resonances as the radiative and bound (non-radiative) modes.

The radiative FB modes occur in subwavelength films at slightly lower wavelengths than the ENZ point and to the left of the light line. This allows the advantageous coupling of light from free space without the need of a special geometry or pattern [24, 62]. Coupling generally requires the incident wavevector to have a nonzero transverse component and is achieved in configurations where a subwavelength ENZ film lies on top of another medium acting as a back-reflector. The phenomenon is named after R. A. Ferrell [79] who showed an absorption peak near the plasma frequency for thin plasmonic films and D. W. Berreman [80] who showed a similar absorption for phononic thin films near the longitudinal phononic resonance that occurs in the optical frequency range.

The bound ENZ mode occurs on the right side of the light line and is therefore not accessible via direct optical excitation. A common configuration to excite ENZ modes is to use the Kretschmann geometry [82–85] where a prism is placed on an ENZ film. The refractive index and incident angle into the prism are used to match the projection of the light momentum along the interface to the ENZ dispersion. This meets the phase-matching condition and excites the ENZ mode. Gratings are also used in a similar capacity to meet the phase-matching conditions [24]. In the literature, the static characteristics of the FB and ENZ modes have been studied in detail [72, 84, 86, 87]. Here, we focus on the modulation around those modes with optical pumping.

4.1 Thin ENZ film on glass

First, we consider a 40 nm ENZ film deposited on glass (Fig. 4a, inset). In this configuration, the film supports a radiative mode that can be excited directly by light from free space. The steady-state absorption in Fig. 4a has a peak slightly to the left of the ENZ point. The large absorption leads to a local minimum in the transmittance at the ENZ point similar to the schematic in Fig. 1c. Therefore, non-monotonic behavior is expected when measuring the transmittance at the ENZ point. A monotonically increasing pump fluence can result in a sign reversal of the transmittance modulation.

An interesting example is found by inspecting at the 60° angle of incidence shown in Fig. 4b–d. Some wavelengths have monotonic behavior when the colors from blue to red do not overlap. For example, at the ENZ wavelength for both transmittance plots (Fig. 4c, d), the modulation increases monotonically with increasing pump fluence. At other wavelengths, the colors overlap showing a non-monotonic behavior. Examples of this are seen at the ENZ wavelength for reflectance and the dashed lines in the transmittance plots (see insets). The sign reversal of the optical response can have an important impact when trying to retrieve optical properties from experimental

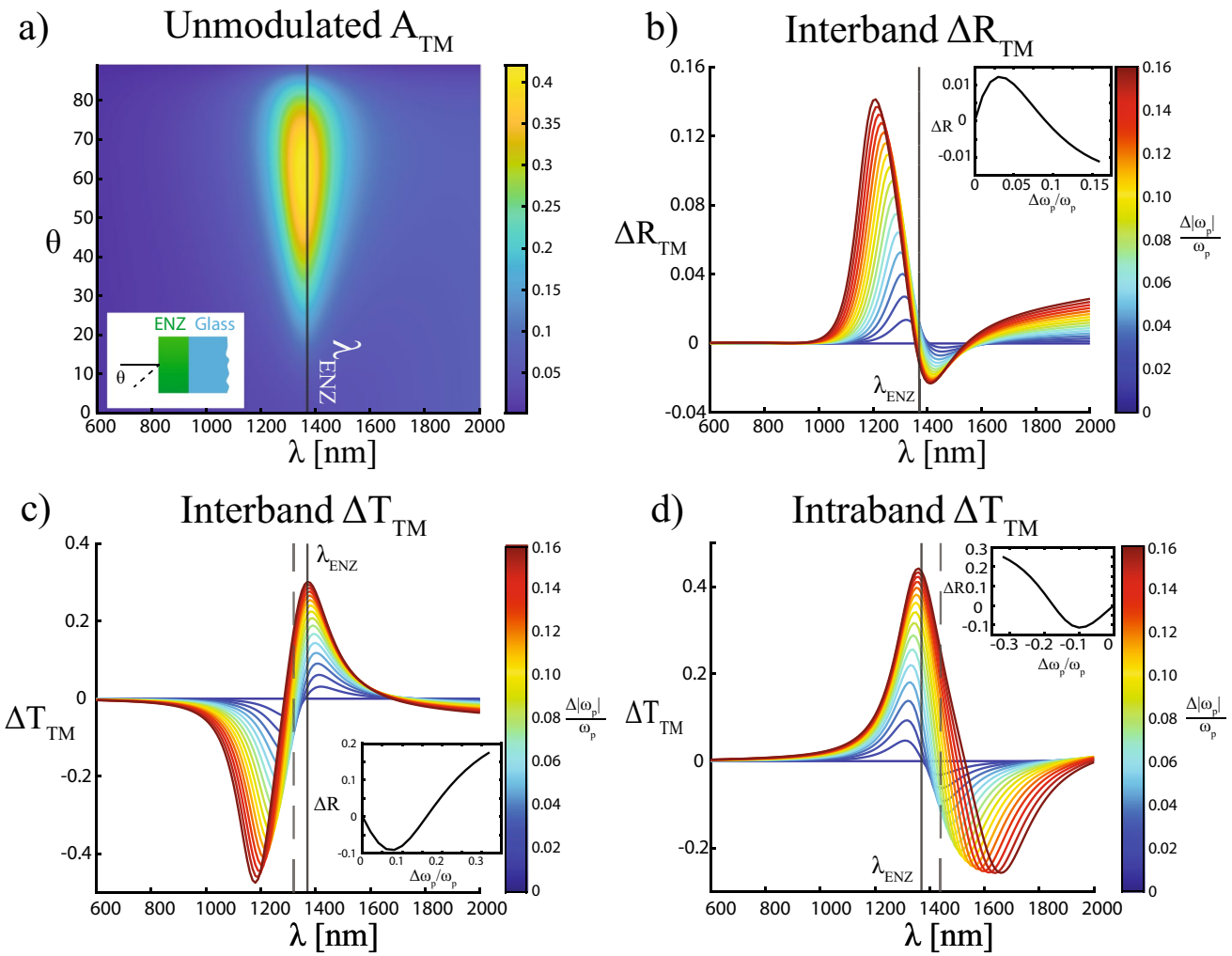

Fig. 4 **a** TM absorptance as a function of wavelength and incident angle. **b** TM reflectance change for interband pumping at 60° incident angles for 40 nm-thick ENZ material on glass substrate. The inset shows the reflection modulation at the ENZ point. The colors represent the magnitude of relative plasma frequency modulation. **c** TM transmittance modulation for interband pumping. The inset displays the transmission along the dashed line $\lambda = 1320$ nm, showing non-monotonous change. The transmittance modulation in ENZ in this case will increase monotonically. **d** The TM transmittance modulation for intraband pumping. The modulation for the dashed line at 1440 nm is plotted in the inset

data. Especially, for nonlinear processes, it is common to measure reflectance/transmittance and then recover the nonlinear susceptibility from those measurements [27, 88]. A sign reversal might then be erroneously attributed to an incorrect sign of the susceptibility.

We appraise this configuration for it prospects in optical switching by evaluating the modulation depth and maximum relative modulation. The steady-state reflectance is small for all angles, because the thin ENZ film does not reflect much light and glass is also transparent. Therefore, reflectance is a poor choice for optical switching, because the depth of modulation is small. This is evident when investigating the steady-state reflectance at the ENZ point, where $R_{TM} \sim 0.1$ and the maximum modulation is $\Delta R_{\mathrm{TM}} \sim 0.01$ (Fig. 4b inset). The transmittance cases show a larger change of nearly $\Delta T_{TM} \sim 0.5$ at selected wavelengths. However, the unmodulated transmittance at 60° is $T_{\mathrm{TM}} \sim 0.5$, making the relative change small. Transmittance is the better of the two, but does not meet both the criteria of large relative change ($\Delta T_{\mathrm{TM}}/T_{\mathrm{TM}} \gg 1$) and a large depth of modulation ($\Delta T_{\mathrm{TM}} \sim 1$).

4.2 Thin ENZ film on metal

Another common experimental configuration is a thin layer of ENZ material deposited on a metal substrate [23, 25, 38, 84, 89](Fig. 5a). The Drude model is used here to describe the metal substrate with the parameters shown in Table 2. This is another example of a radiative mode where a large absorption peak exists near the ENZ point. The

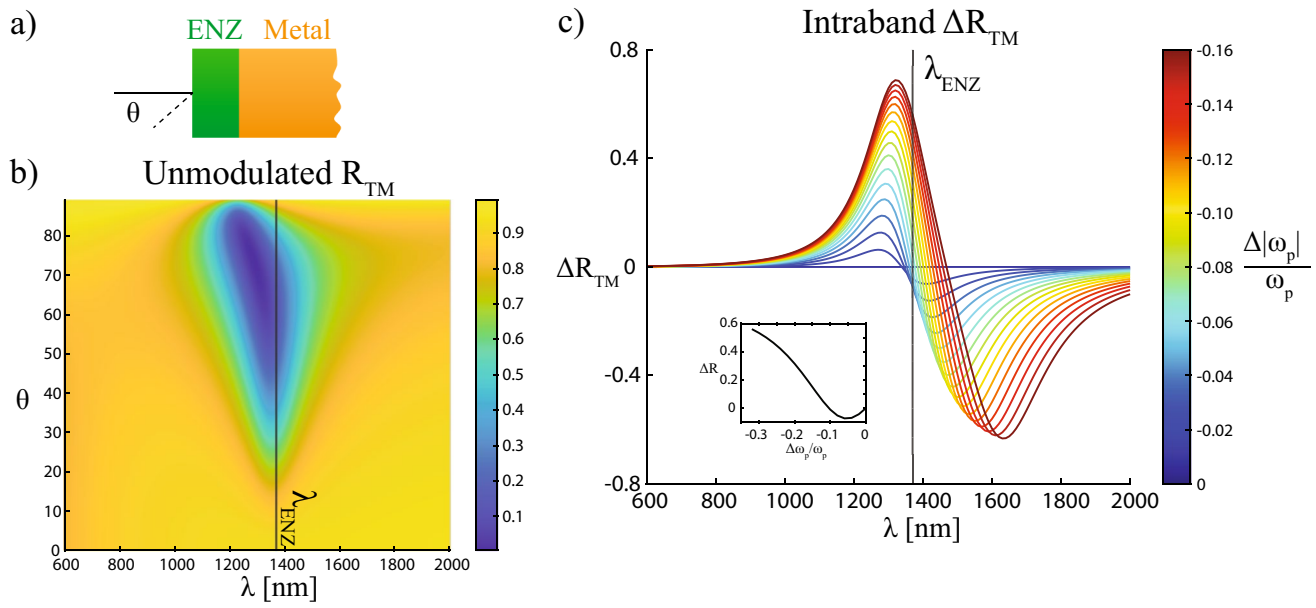

Fig. 5 **a** Configuration schematic. **b** Unmodulated TM reflectance as a function of wavelength and incident angle for 10 nm ENZ film on a metal substrate. **c** Modulated absolute TM reflectance for intraband pumping at 60° incident angle. The Drude parameters for the metal can be found in Table 2. The inset of **c** shows the trend of reflectance at the ENZ point

transmittance in this case is negligible and the reflectance is high because of the metal layer. The reflectance shows a dip where the absorption is the highest (Fig. 5b) that can be used for optical switching. The reflectance dip follows parallel to ENZ wavelength for lower incident angles and diverges to the ENZ–metal surface polariton resonance at higher angles. The offset of the minimum from the ENZ wavelength causes a probe at the ENZ wavelength to experience non-monotonic reflectance for intraband pumping (Fig. 5c inset).

The large contrast of the reflectance dip motivates the use of this configuration for all-optical switching and both interband and intraband pumping are applicable. For larger angles of incidence ($\theta > 60$), the reflectance dip is not symmetric around the minimum; therefore, interband and intraband pumping require different intensities to achieve the same switching contrast. Intraband pumping is then slightly favorable, because the transition from low to high reflectance happens over a shorter wavelength range requiring less modulation of the plasma frequency.

Comparing the absolute reflectance change in Fig. 5c to the changes in Fig. 4, we see a larger absolute modulation for improved switching. At some wavelengths $|\Delta R_{\mathrm{TM}}| > 0.6$, such as at $\lambda = 1320$ nm where the relative reflectance change is approximately ten times. Both the relative change and the modulation depth are large here making this configuration a better candidate for switching (recall that reflectance and transmittance are scaled to one). This also illustrates how the ENZ wavelength is not always the best suited for all-optical switching, since the largest modulation for 60° angle of incidence is at $\lambda = 1320$ nm and the ENZ wavelength is $\lambda_{\mathrm{ENZ}} = 1380$ nm.

The FB mode illustrated in this example has been used for femtosecond polarization switching by Yang et al.[38]. A linearly polarized probe beam with both TE and TM components was incident on doped CdO deposited on gold and a pump beam was used to modulate the ENZ point. The reflectance was modulated from $R_{\mathrm{TM}} = 0.01$ to $R_{\mathrm{TM}} = 0.86$ in the TM component, while the TE component had no observable modulation. Taking advantage of the different absorptance for TE and TM polarized light near the ENZ point, an optically controlled polarization switch was demonstrated by either increasing or decreasing attenuation of the reflected TM light.

4.3 The ENZ mode

Exciting the ENZ mode requires a special geometry such as the Kretschmann geometry using a prism. For our calculations, we assume that a prism with a refractive index of 1.95 is placed on a 10 nm ENZ film on a glass

Table 2 Optical properties of hypothetical metal

Drude model parameters	Value
$\varepsilon_{\mathrm{metal}}$	3.5
$\omega_{\mathrm{P_{metal}}}$	9.6×10^{15} rad/s
Γ_{metal}	$4.8 \times 10^{13} s^{-1}$

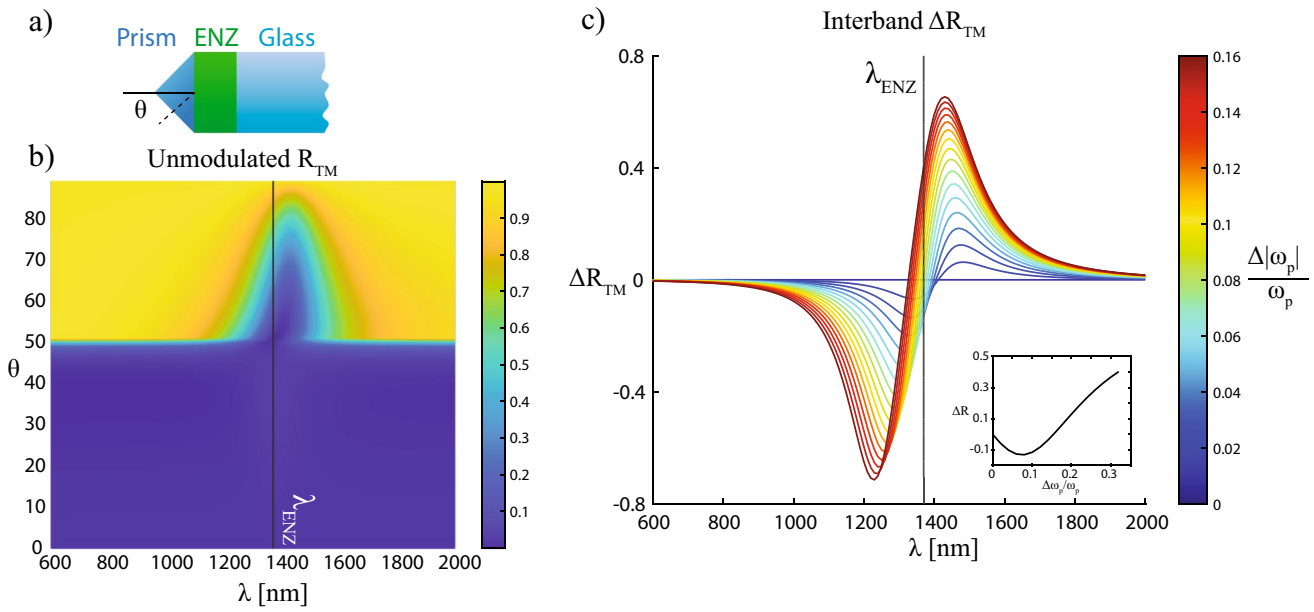

Fig. 6 **a** Experimental configuration. A prism ($n_{prism} = 1.95$) is placed on top of a 10 nm ENZ film which is deposited on glass ($n_{glass} = 1.5$). **b** Unmodulated TM reflectance for the Kretschmann geometry. **c** Modulated absolute TM reflectance for interband pumping at 60° incident angle. The inset shows the modulation trend at the ENZ point as the modulation is increased

substrate ($n_{glass} = 1.5$). A schematic of the configuration is shown in Fig. 6a, where angle of incidence is defined with respect to the normal of ENZ film and not the prism, to make comparing with previous examples easier. The ENZ layer needs to be deeply subwavelength to observe the ENZ mode [72] and because of that a clear line at approximately 50° shows the total reflection angle corresponding to the prism-glass critical angle. At angles larger than 50°, the ENZ mode is visible as a dip in the reflectance spectrum (Fig. 6b). Investigating again along the 60° angle of incidence (to compare with previous cases), we see a similar amount of modulation in the reflectance as in the FB mode. In contrast, the dip in this case is at larger wavelengths than the ENZ point, where for the FB mode, it is at smaller wavelengths. Therefore, the ENZ mode is equally viable as an optical switch compared to the FB mode.

A similar configuration was utilized by Bohn et al., where a 60 nm ITO film was placed on a prism and exposed to air. Using the coupling between pump and probe beam they reported reflectance changing from $R_{TM} = 0.01$ to $R_{TM} = 0.45$ with ultrafast switching speeds [62]. By probing away from the reflectance minimum, they also observed the ultrafast non-monotonic behavior of reflectance as the pump pulse shifted the reflectance minimum through the probe wavelength. This exact behavior is seen in the inset of Fig. 6c, where a sweeping of modulation intensity shows first a decrease, and then increase in reflectance. This brings about an important point that the ENZ modulation may not be monotonic during the interaction with a pulsed laser as intensity ramps up. This is especially important for cases where the probe-pulse duration is less than the pump-pulse duration, which is often true for pump-probe experiments.

5 Effect of Drude-damping factor and energy dissipation

In the previous examples, we assumed that photoexcitation of free carriers only changed the plasma frequency by increasing the free-carrier concentration or their effective mass. However, damping also plays an important role in all-optical switching. The damping factor represents the inverse of the scattering time for free electrons and is therefore related to the electron density [90]. Optical pumping has been shown to change the damping factor [38, 63, 68, 91, 92], and depending on experimental factors, it can either decrease or increase.

The resulting change in damping factor due to optical pumping modulates the ENZ point. Re-examining the ENZ frequency derived from Eq. (2) while including the effect of damping results with $\omega_{ENZ} = \sqrt{\omega_p^2/\varepsilon_\infty - \Gamma_0^2}$. We can estimate the size of this effect by comparing terms under the square-root sign. For typical experimental values, $\Gamma_0/\omega_p \leq 1/10$ and the correction is small. There is a stronger effect from damping changes on the ENZ resonance width.

An illustrative example is made by examining the spectral width change for a thin ENZ layer like that in Fig. 4. We considered three cases of differing damping constants shown in Fig. 7, where all other parameters are the same as in the thin ENZ case. We plot the steady-state transmission of TM polarized light through the thin film showing drastic changes in the resonance width with varying damping factors; careful inspection also reveals a shift in the absorption peak indicating a change in the ENZ point.

The immediate conclusion from this example with regards to ultrafast optical switching is the need to keep the damping constant small for a narrow resonance. A narrow resonance allows for sharper changes in the transmittance and reflectance, at lower pumping intensities. For example, if we consider the 60° incidence angle, the half width of the transmission dip is ~ 80 nm for the case of Fig. 7a. The unmodulated transmittance is $T_{TM} \sim 0.04$. Using a plasma frequency modulation of $\Delta\omega_p/\omega_p = 0.15$, the transmittance increases by 20 times. In contrast, for the same plasma frequency modulation, the change in the case of Fig. 7b is at most a factor of two and less than one-tenth change for Fig. 7c. The losses should then be tailored to accommodate the switching specifications. Low losses should be used for efficient narrow-band switches, while moderate losses may be more applicable for broadband switching.

6 Outlook

In this tutorial, we study the modulation of the reflectance and transmittance of various ENZ media, with interband and intraband optical pumping using the Drude model. We discuss the effects of pumping on the plasma frequency and employed the TMM to analyze experimental configurations. The cases studied here point out general aspects for all-optical switching with ENZ materials. First, the use of ENZ materials greatly increases the modulation of the refractive index. Second, thin films demonstrate absorption peaks near the ENZ wavelength because of the strong interaction between surface waves. The absorption peaks imply a dip in transmittance or reflectance that can be shifted with optical pumping. This causes substantial changes in the reflectance or transmittance allowing such systems to be utilized for all-optical switching. Finally, losses due to damping affect the ENZ point and the resonance width. There is a trade-off where larger damping factors broaden the resonance allowing for broadband switching. However, the depth of the absorption is reduced and makes the contrast between switching states smaller. Oppositely, lower damping factors have a narrower resonance that reduces the optical switch bandwidth, but increases the switch contrast.

We also show that although the largest modulations occur proximal to the ENZ point, the ENZ point itself is not always the best wavelength for optical switching. For example, the Ferrell–Berreman mode or ENZ mode are excited above and below the ENZ wavelength, respectively, resulting in the maximum modulation occurring away from ENZ point. Deviations of the wavelength away from the maximum/minimum results in a non-monotonic trend of the reflectance or transmittance as a function of the optical pumping power. Therefore, it is critical to optically characterize ENZ materials in the steady state, so that the unpumped ENZ point and nearby resonances are well identified. The pump power along with the pump photon energy are also important parameters in experiments. These effects should be carefully considered, especially when tracking the changes in reflectance or transmittance to extract the optical properties in the photoexcited state.

Throughout, we have discussed multiple common experimental configurations and ENZ schemes, focusing on all-optical switching. These configurations are building blocks for understanding and constructing more complex experiments such as those involving time refraction [55],

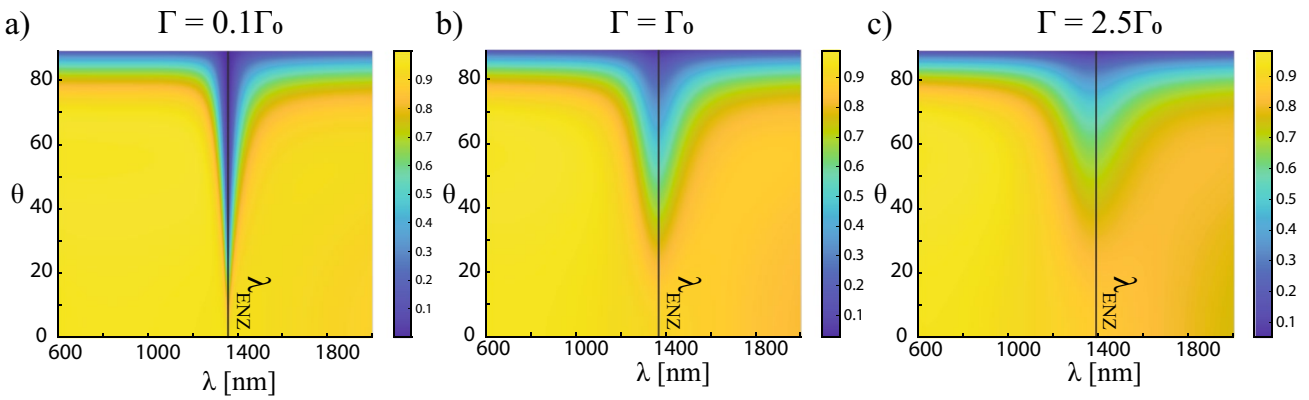

Fig. 7 Transmission of a thin (40 nm) ENZ film deposited on glass. Same conditions as Fig. 4, except for the damping factor, which is **a** $\Gamma = 0.1\Gamma_0$, **b** $\Gamma = \Gamma_0$, and **c** $\Gamma = 2.5\Gamma_0$, where Γ_0 can be found in Table 1

time reflection [57], negative refraction [56], and four-wave mixing [93], where the ultrafast refractive index transitions from optical switches may be used.

Acknowledgements This tutorial includes work that was supported by the U.S. Department of Energy, Office of Basic Energy Sciences, Division of Materials Sciences and Engineering under Award DE-SC0017717, the Office of Naval Research under Award N00014-20-1-2199, and the Air Force Office of Scientific Research under Award FA9550-18-1-0002.

References

1. M. Reutzel, A. Li, B. Gumhalter, H. Petek, Phys. Rev. Lett. **123**, 017404 (2019)
2. P.B. Johnson, R.W. Christy, Phys. Rev. B **9**, 5056 (1974)
3. P.B. Johnson, R.W. Christy, Phys. Rev. B **6**, 4370 (1972)
4. G.V. Naik, V.M. Shalaev, A. Boltasseva, Adv. Mater. **25**, 3264 (2013)
5. N. Kinsey, C. DeVault, J. Kim, M. Ferrera, V.M. Shalaev, A.A. Boltasseva, Optica **2**, 616 (2015)
6. T. Tyborski, S. Kalusniak, S. Sadofev, F. Henneberger, M. Woerner, T. Elsaesser, Phys. Rev. Lett. **115**, 147401 (2015)
7. M.Z. Alam, I. de Leon, R.W. Boyd, Science **352**, 795 (2016)
8. A. Ciattoni, C. Rizza, E. Palange, Phys. Rev. A **81**, 043839 (2010)
9. C. Argyropoulos, P.Y. Chen, G. D'Aguanno, N. Engheta, A. Alù, Phys. Rev. B Condens. Matter and Mater. Phys. **85**, 45129 (2012)
10. B. Edwards, A. Alù, M.E. Young, M. Silveirinha, N. Engheta, Phys. Rev. Lett. **100**, 1 (2008)
11. G. Subramania, A.J. Fischer, T.S. Luk, Appl. Phys. Lett. **101**, 241107 (2012)
12. R. Maas, J. Parsons, N. Engheta, A. Polman, Nat. Photon. **7**, 907 (2013)
13. A.A. Basharin, C. Mavidis, M. Kafesaki, E.N. Economou, C.M. Soukoulis, Phys. Rev. B Condens. Matter Mater. Phys. **87**, 155130 (2013)
14. S. Suresh, O. Reshef, M.Z. Alam, J. Upham, M. Karimi, R.W. Boyd, ACS Photon. **8**, 125 (2021)
15. Y. Li, C.T. Chan, E. Mazur, Light Sci. Appl. **10**, 203 (2021)
16. D.I. Vulis, P. Camayd-Muñoz, Y. Li, O. Reshef, M. Lončar, E. Mazur, Integrated zero-index supercouplers. Frontiers in Optics 2017, (Optical Society of America, 2017) pp JW3A.108. http://opg.optica.org/abstract.cfm?URI=LS-2017-JW3A.108
17. M. Silveirinha, N. Engheta, Phys. Rev. Lett. **97**, 157403 (2006)
18. M.G. Silveirinha, N. Engheta, Phys. Rev. B Condens. Matter Mater. Phys. **76**, 245109 (2007)
19. S. Enoch, G. Tayeb, P. Sabouroux, N. Guérin, P. Vincent, Phys. Rev. Lett. **89**, 603 (2002)
20. G. Lovat, P. Burghignoli, F. Capolino, D.R. Jackson, and D.R. Wilton, Directive radiation from a line source in a metamaterial slab with low permittivity. 2005 IEEE Antennas and Propagation Society International Symposium, vol 1B (Digest), pp 260–263 (2005). https://doi.org/10.1109/APS.2005.1551537
21. A. Alù, M.G. Silveirinha, A. Salandrino, N. Engheta, Phys. Rev. B Condens. Matter Mater. Phys. **75**, 155410 (2007)
22. A. Monti, F. Bilotti, A. Toscano, L. Vegni, Opt. Commun. **285**, 3412 (2012)
23. T.S. Luk, S. Campione, I. Kim, S. Feng, Y.C. Jun, S. Liu, J.B. Wright, I. Brener, P.B. Catrysse, S. Fan, M.B. Sinclair, Phys. Rev. B Condens. Matter Mater. Phys. **90**, 085411 (2014)
24. J. Park, J.H. Kang, A.P. Vasudev, D.T. Schoen, H. Kim, E. Hasman, M.L. Brongersma, ACS Photon. **1**, 812 (2014)
25. J. Rensberg, Y. Zhou, S. Richter, C. Wan, S. Zhang, P. Schöppe, R. Schmidt-Grund, S. Ramanathan, F. Capasso, M.A. Kats, C. Ronning, Phys. Rev. Appl. **8**, 014009 (2017)
26. A. Marini, F.J. Garcia De Abajo, Sci. Rep. **6**, 20088 (2016)
27. L. Caspani, R.P.M.M. Kaipurath, M. Clerici, M. Ferrera, T. Roger, J. Kim, N. Kinsey, M. Pietrzyk, A. di Falco, V.M. Shalaev, A. Boltasseva, D. Faccio, Phys. Rev. Lett. **116**, 233901 (2016)
28. M.Z. Alam, S.A. Schulz, J. Upham, I. de Leon, R.W. Boyd, Nat. Photon. **12**, 79 (2018)
29. K. Wu, Z. Wang, J. Yang, H. Ye, Opt. Lett. **44**, 2490 (2019)
30. I. Liberal, N. Engheta, Nat. Photon. **11**, 149 (2017)
31. X. Niu, X. Hu, S. Chu, Q. Gong, Adv. Opt. Mater. **6**, 1701292 (2018)
32. N. Kinsey, C. DeVault, A. Boltasseva, V.M. Shalaev, Nat. Rev. Mater. **4**, 742 (2019)
33. O. Reshef, I. de Leon, M.Z. Alam, R.W. Boyd, Nat. Rev. Mater. **4**, 535 (2019)
34. J. Wu, Z.T. Xie, Y. Sha, H.Y. Fu, Q. Li, Photon. Res. **9**, 1616 (2021)
35. A. Boltasseva, H.A. Atwater, Science **331**, 290 (2011)
36. G.V. Naik, J. Kim, A. Boltasseva, Opt. Mater. Express **1**, 1090 (2011)
37. M. Clerici, N. Kinsey, C. DeVault, J. Kim, E.G. Carnemolla, L. Caspani, A. Shaltout, D. Faccio, V. Shalaev, A. Boltasseva, M. Ferrera, Nat. Commun. **8**, 15829 (2017)
38. Y. Yang, K. Kelley, E. Sachet, S. Campione, T.S. Luk, J.P. Maria, M.B. Sinclair, I. Brener, Nat. Photon. **11**, 390 (2017)
39. S. Gurung, A. Anopchenko, S. Bej, J. Joyner, J.D. Myers, J. Frantz, H.W.H. Lee, Atomic Layer Engineering of Epsilon-Near-Zero Ultrathin Films with Controllable Field Enhancement. Adv. Mater. Interfaces **7**(17), 2000844 (Wiley Online Library, 2020)
40. S. Saha, B.T. Diroll, J. Shank, Z. Kudyshev, A. Dutta, S.N. Chowdhury, T.S. Luk, S. Campione, R.D. Schaller, V.M. Shalaev, A. Boltasseva, M.G. Wood, Adv. Funct. Mater. **30**, 1908377 (2020)
41. H. Zhao, Y. Wang, A. Capretti, L. Dal Negro, J. Klamkin, IEEE J. Sel. Top. Quantum Electron. **21**, 192 (2015)
42. J.W. Cleary, E.M. Smith, K.D. Leedy, G. Grzybowski, J. Guo, Opt. Mater. Express **8**, 1231 (2018)
43. Y. Wang, A.C. Overvig, S. Shrestha, R. Zhang, R. Wang, N. Yu, L. Dal Negro, Opt. Mater. Express **7**, 2727 (2017)
44. M. Abb, P. Albella, J. Aizpurua, O.L. Muskens, Nano Lett. **11**, 2457 (2011)
45. A. Capretti, L.D. Negro, N. Engheta, Y. Wang, Opt. Lett. **40**(7), 1500–1503 (2015)
46. J. Wu, Z. T. Xie, H. Y. Fu, and Q. Li, in 2020 12th International Conference on Advanced Infocomm Technology, ICAIT 2020, p. 5 (2020)
47. W. Tian, F. Liang, D. Lu, H. Yu, H. Zhang, Photon. Res. **9**, 317 (2021)
48. J. Kim, A. Dutta, G.V. Naik, A.J. Giles, F.J. Bezares, C.T. Ellis, J.G. Tischler, A.M. Mahmoud, H. Caglayan, O.J. Glembocki, A.V. Kildishev, J.D. Caldwell, A. Boltasseva, N. Engheta, Optica **3**, 339 (2016)
49. C. DeVault, V.A. Zenin, A. Pors, J. Kim, K. Chaudhuri, S. Bozhevolnyi, V.M. Shalaev, and A. Boltasseva, Plasmonic antenna resonance pinning and suppression of near-field coupling from epsilon-near-zerosubstrate. 2017 Conference on Lasers and Electro-Optics, CLEO 2017-Proceedings, pp. 1–1 (2017)
50. C.T. DeVault, V.A. Zenin, A. Pors, K. Chaudhuri, J. Kim, A. Boltasseva, V.M. Shalaev, S.I. Bozhevolnyi, Optica **5**, 1557 (2018)
51. S.A. Schulz, A.A. Tahir, M.Z. Alam, J. Upham, I. de Leon, R.W. Boyd, Phys. Rev. A **93**, 063846 (2016)
52. S. Vezzoli, V. Bruno, C. Devault, T. Roger, V.M. Shalaev, A. Boltasseva, M. Ferrera, M. Clerici, A. Dubietis, D. Faccio, Phys. Rev. Lett. **120**, 43902 (2018)

53. J.B. Khurgin, M. Clerici, V. Bruno, L. Caspani, C. DeVault, J. Kim, A. Shaltout, A. Boltasseva, V.M. Shalaev, M. Ferrera, D. Faccio, N. Kinsey, Optica **7**, 226 (2020)
54. K. Pang, M.Z. Alam, Y. Zhou, C. Liu, O. Reshef, K. Manukyan, M. Voegtle, A. Pennathur, C. Tseng, X. Su, H. Song, Z. Zhao, R. Zhang, H. Song, N. Hu, A. Almaiman, J.M. Dawlaty, R.W. Boyd, M. Tur, A.E. Willner, Nano Lett. **21**, 5907 (2021)
55. Y. Zhou, M.Z. Alam, M. Karimi, J. Upham, O. Reshef, C. Liu, A.E. Willner, R.W. Boyd, Nat. Commun. **11**, 2180 (2020)
56. V. Bruno, C. DeVault, S. Vezzoli, Z. Kudyshev, T. Huq, S. Mignuzzi, A. Jacassi, S. Saha, Y.D. Shah, S.A. Maier, D.R.S. Cumming, A. Boltasseva, M. Ferrera, M. Clerici, D. Faccio, R. Sapienza, V.M. Shalaev, Phys. Rev. Lett. **124**, 043902 (2020)
57. E. Lustig, Y. Sharabi, M. Segev, Optica **5**, 1390 (2018)
58. J.B. Khurgin, M. Clerici, N. Kinsey, Laser Photon. Rev. **15**, 2000291 (2021)
59. J.B. Khurgin, Adv. Opt. Photon. **2**, 287 (2010)
60. N. Kinsey, J. Khurgin, Optical Materials Express **9**, 2793 (2019)
61. B.T. Diroll, S. Saha, V.M. Shalaev, A. Boltasseva, R.D. Schaller, Adv. Opt. Mater. **8**, 2000652 (2020)
62. J. Bohn, T.S. Luk, C. Tollerton, S.W. Hutchings, I. Brener, S. Horsley, W.L. Barnes, E. Hendry, Nat. Commun. **12**, 1017 (2021)
63. S. Saha, A. Dutta, C. DeVault, B.T. Diroll, R.D. Schaller, Z. Kudyshev, X. Xu, A. Kildishev, V.M. Shalaev, A. Boltasseva, Mater. Today **43**, 27 (2021)
64. V.E. Babicheva, A. Boltasseva, A.V. Lavrinenko, Nanophotonics **4**, 165 (2015)
65. A.D. Dunkelberger, D.C. Ratchford, A.B. Grafton, V.M. Breslin, E.S. Ryland, D.S. Katzer, K.P. Fears, R.J. Weiblen, I. Vurgaftman, A.J. Giles, C.T. Ellis, J.G. Tischler, J.D. Caldwell, J.C. Owrutsky, ACS Photon. **7**, 279 (2020)
66. R. Secondo, J. Khurgin, N. Kinsey, Opt. Mater. Express **10**, 1545 (2020)
67. A.R. Rashed, B. Can Yildiz, S.R. Ayyagari, H. Caglayan, Phys. Rev. B **101**, 1301 (2020)
68. H. Wang, K. Du, X. Dai, W. Zhang, R. Liu, S.J. Chua, T. Mei, Nanophotonics **9**, 4287 (2020)
69. Q. Guo, Y. Cui, Y. Yao, Y. Ye, Y. Yang, X. Liu, S. Zhang, X. Liu, J. Qiu, H. Hosono, Adv. Mater. **29**, 1700754 (2017)
70. H. George, J. Reed, M. Ferdinandus, C. DeVault, A. Lagutchev, A. Urbas, T.B. Norris, V.M. Shalaev, A. Boltasseva, N. Kinsey, Opt. Mater. Express **9**, 3911 (2019)
71. B.E.A. Saleh, M.C. Teich, *Fundamentals of photonics* (Wiley, Berlin, 2019)
72. S. Campione, I. Brener, F. Marquier, Phys. Rev. B Condens. Matter Mater. Phys. **91**, 1408 (2015)
73. S. Campione, I. Kim, D. de Ceglia, G.A. Keeler, T.S. Luk, Opt. Express **24**, 18782 (2016)
74. G.H. Meeten, Meas. Sci. Technol. **8**, 728 (1997)
75. K.L. Kliewer, R. Fuchs, Phys. Rev. **153**, 498 (1967)
76. D. Traviss, R. Bruck, B. Mills, M. Abb, O.L. Muskens, Appl. Phys. Lett. **102**, 1212 (2013)
77. K. Chaudhuri, U. Guler, S.I. Azzam, H. Reddy, S. Saha, E.E. Marinero, A.V. Kildishev, V.M. Shalaev, A. Boltasseva, ACS Photon. **7**, 472 (2020)
78. P. Berini, Adv. Opt. Photon. **1**, 484 (2009)
79. R.A. Ferrell, Phys. Rev. **111**, 1214 (1958)
80. D.W. Berreman, Phys. Rev. **130**, 2193 (1963)
81. W.D. Newman, C.L. Cortes, J. Atkinson, S. Pramanik, R.G. Decorby, Z. Jacob, ACS Photon. **2**, 2 (2015)
82. E. Kretschmann, H. Raether, Z. Für Naturforschung A **23**, 2135 (1968)
83. A. Otto, E. Burstein, F. Demartina, The surface polariton response in attenuated total reflection. In: Polaritons: Proceedings of the First Taormina Research Conference on the Structure of Matter, (Pentagon, New York, 1974), pp. 117–121
84. A. Anopchenko, L. Tao, C. Arndt, H.W.H. Lee, ACS Photon. **5**, 2631 (2018)
85. A.P. Vinogradov, A.V. Dorofeenko, A.A. Pukhov, A.A. Lisyansky, Phys. Rev. B **97**, 235407 (2018)
86. S. Vassant, J.-P. Hugonin, F. Marquier, J.-J. Greffet, Opt. Express **20**, 23971 (2012)
87. E.L. Runnerstrom, K.P. Kelley, E. Sachet, C.T. Shelton, J.P. Maria, ACS Photon. **4**, 1885 (2017)
88. E.G. Carnemolla, L. Caspani, C. DeVault, M. Clerici, S. Vezzoli, V. Bruno, V.M. Shalaev, D. Faccio, A. Boltasseva, M. Ferrera, Opt. Mater. Express **8**, 3392 (2018)
89. Y. Yang, J. Lu, A. Manjavacas, T.S. Luk, H. Liu, K. Kelley, J.P. Maria, E.L. Runnerstrom, M.B. Sinclair, S. Ghimire, I. Brener, Nat. Phys. **15**, 1022 (2019)
90. D. Puerto, J. Siegel, W. Gawelda, M. Galvan-Sosa, L. Ehrentraut, J. Bonse, J. Solis, J. Opt. Soc. Am. B **27**, 1065 (2010)
91. R.J. Kirby, A. Ferrenti, C. Weinberg, S. Klemenz, M. Oudah, S. Lei, C.P. Weber, D. Fausti, G.D. Scholes, L.M. Schoop, J. Phys. Chem. Lett. **11**, 6105 (2020)
92. J. Kuttruff, D. Garoli, J. Allerbeck, R. Krahne, A. de Luca, D. Brida, V. Caligiuri, N. Maccaferri, Commun. Phys. **3**, 114 (2020)
93. V. Bruno, S. Vezzoli, C. DeVault, E. Carnemolla, M. Ferrera, A. Boltasseva, V.M. Shalaev, D. Faccio, M. Clerici, C. de Vault, E. Carnemolla, M. Ferrera, A. Boltasseva, V.M. Shalaev, D. Faccio, M. Clerici, Appl. Sci. **10**, 1318 (2020)